PERGAMON

International Journal of Solids and Structures 36 (1999) 5467–5484

INTERNATIONAL JOURNAL OF SOLIDS and STRUCTURES

www.elsevier.com/locate/ijsolstr

Transient dynamic response of piezoelectric bodies subjected to internal electric impulses

Horacio Sosa*, Naum Khutoryansky

Department of Mechanical Engineering and Mechanics, Drexel University, Philadelphia, PA 19104, U.S.A.

Received 12 April 1998

Abstract

The response of piezoelectric bodies disturbed by internal electric sources is investigated using integral representations of Green's functions and their derivatives. The emphasis of the article is placed on transient dynamic phenomena promoted by high intensity electric discharges applied over very short intervals of time. To that end closed form integral representations of the electro-elastic variables are derived and applied to investigate the behavior of transversely isotropic piezoelectric ceramics. In particular, the characteristics of the induced stress and electric field components are investigated numerically for the case of charge impulses of triangular shape.

1. Introduction

Piezoelectric ceramics are used in modern technologies to convert mechanical energy into electrical energy and vice versa. Examples illustrating the use of these materials include multilayer electromechanical devices, electronic components, micromechanical systems and sensors and actuators embedded in intelligent structures. In these and other applications the mechanical and electrical reliability of the ceramic as well as the durability of the device or structure are issues of great concern. Indeed, loading conditions of mechanical, thermal and electrical nature tend to produce stresses and electric fields of magnitudes large enough to cause depoling, dielectric breakdown and even catastrophic failure (Freiman and Pohanka, 1989).

During the past ten years there has been a good number of electro-elastic models developed to describe the behavior of piezoceramics weakened by defects such as cracks and cavities (see e.g. McMeeking, 1987; Pak, 1990; Sosa, 1991, 1992; Sosa and Khutoryansky, 1996; Suo, 1993 and references therein). Most of the advances have been based on a generalization of fracture mechanics concepts to incorporate the effects of the electrical variables. In general, one can say that the outcomes from those models have been quite satisfactory: there is a better understanding of how

* Corresponding author. Fax: 215 895 1478

0020-7683/99/$ - see front matter
PII: S0020-7683(98)00246-7

electric fields are perturbed in the presence of defects; it is now clear that cracks can be stopped if a voltage is applied in a particular direction; and there is conclusive theoretical proof that boundary conditions influence the qualitative behavior of fields int he neighborhood of crack tips.

On the other hand, little is known on the effects that phenomena of impulsive nature have on the behavior of piezoceramics. In fact, devices such as phase change transducers, pulse generators for igniters and high voltage transformers are almost routinely subjected to very large voltages over very short intervals of time. While these disturbances may dissipate rather quickly, they can nevertheless promote failure if the propagating electric and acoustic waves encounter voids, cracks, impurities or any other surface of discontinuity-like embedded electrodes.

The present article is a sequel to a previous paper (Khutoryansky and Sosa, 1995) on the transient dynamic response of piezoelectric ceramics, where dynamic fundamental solutions (Green's functions) were derived and represented in three different manners to describe the characteristics of electro-elastic variables. These three alternative representations are again presented but rewritten in a more convenient form to address the problem of interest in this article, namely the case of bodies subjected to electric pulses of arbitrary shape. In addition, a thorough discussion on the representation of fundamental solutions via slowness surfaces is provided. From both a theoretical and computational point of view, the most important aspect of the article is rendering one-dimensional integral representations for the field variables in a rather simple form, despite the physical complexities of the problems under study. Thus, a numerical example is provided for a particular class of piezoceramic to illustrate the virtues of such a representation. The results disclose interesting material phenomena, otherwise difficult to deduce on physical grounds or difficult to reproduce in the laboratory.

2. Dynamic Green's functions

Both direct and component notation within the framework of Cartesian coordinates is used throughout. Tensors of rank one and above as well as their matrix representations are denoted by bold face letters. In the case of component notation we invoke the summation convention over repeated lower and upper case Latin subindices with the following ranges: $i, j, k, \cdots = 1, 2, 3$ and $K, L, M, \cdots = 1, 2, 3, 4$.

Let $\mathscr{B}$ denote the piezoelectric body with boundary $\partial\mathscr{B}$, which is assumed homogeneous and governed by

$$\begin{aligned} C_{ijkl}u_{k,lj} + e_{kij}\phi_{,kj} + b_i &= \rho\ddot{u}_i \\ e_{ikl}u_{k,li} - \varepsilon_{ik}\phi_{,ki} &= q \end{aligned} \tag{1}$$

where u_i, ϕ, b_i, ρ and q denote the displacement, electric potential, body force per unit of volume, mass density, and electric charge density, respectively. Moreover, C_{ijkl}, e_{ijk} and ε_{ij} are the elastic (measured at constant electric field), piezoelectric and dielectric (measured at constant strain) constants, respectively, satisfying the following symmetry relations:

$$C_{ijkl} = C_{ijlk} = C_{jikl} = C_{klij}; \quad e_{kij} = e_{kji}; \quad \varepsilon_{ik} = \varepsilon_{ki}$$

The above system of equations must be solved subject to the following boundary conditions:

$$u_i = \bar{u}_i \quad \text{on } \partial\mathscr{B}_u$$

$$\sigma_{ij} v_{ij} = \bar{t}_i \quad \text{on } \partial\mathscr{B}_t$$

$$[\![\phi]\!] = 0 \quad \text{on } \partial\mathscr{B}_\phi$$

$$[\![D_i]\!] v_i = \bar{w}_s \quad \text{on } \partial\mathscr{B}_w \tag{2}$$

and the following initial conditions:

$$u_i(\mathbf{x}, 0) = u_i^0(\mathbf{x})$$

$$\dot{u}_i(\mathbf{x}, 0) = v_i^0(\mathbf{x}) \tag{3}$$

where σ_{ij} is the stress, D_i the induction (or electric displacement), $\bar{u}_i$, $\bar{t}_i$ and $\bar{w}_s$ are prescribed values of displacement, traction and surface charge, respectively, v_i is the outward unit normal to the boundary or interior surface of discontinuity and the symbol $[\![\cdot]\!]$ denotes the jump of the enclosed quantity across the surface. Lastly, $u_i^0(\mathbf{x})$ and $v_i^0(\mathbf{x})$ are prescribed initial values of displacement and velocity.

As mentioned in the introduction, we have derived the fundamental solutions for three-dimensional dynamic piezoelectricity by introducing the matrix of Green's functions $\mathbf{U}$ given by

$$\mathbf{U}(\mathbf{x}, t) = \begin{Vmatrix} U_{ij} & U_{i4} \\ U_{4j} & U_{44} \end{Vmatrix} \tag{4}$$

with the understanding that U_{ij} and U_{4j} represent the displacement (in the i-direction) and the electric potential, respectively, at a field point $\mathbf{x} = \{\mathbf{x}_i\}$ due to a unit force applied at a source point $\xi = \{\xi_i\}$ in the j-direction. Likewise, U_{i4} and U_{44} represent the displacement and electric potential, respectively, at $\mathbf{x}$ when a point charge is applied at ξ.

If we introduce the four-dimensional vectors

$$\mathbf{d} = \begin{Bmatrix} \mathbf{u} \\ \phi \end{Bmatrix}, \quad \mathbf{f} = \begin{Bmatrix} \mathbf{b} \\ -q \end{Bmatrix} \tag{5}$$

and the differential operator

$$\mathbf{L}(\nabla, \partial_t) = \begin{Vmatrix} \rho\, \partial_t^2 & 0 \\ 0 & 0 \end{Vmatrix} - \begin{Vmatrix} \mathbf{A} & \mathbf{a} \\ \mathbf{a}^T & -\alpha \end{Vmatrix} \tag{6}$$

where $\mathbf{A}(\nabla)$, $\mathbf{a}(\nabla)$ and $\alpha(\nabla)$ are tensors of rank two, one and zero, respectively, with components

$$A_{ik} = C_{ijkl} \frac{\partial}{\partial x_j} \frac{\partial}{\partial x_l}, \quad a_i = e_{kij} \frac{\partial}{\partial x_k} \frac{\partial}{\partial x_j}, \quad \alpha = \varepsilon_{ik} \frac{\partial}{\partial x_i} \frac{\partial}{\partial x_k} \tag{7}$$

then (1) can be written as

$$\mathbf{L}(\nabla, \partial_t)\mathbf{d}(\mathbf{x}, t) = \mathbf{f}(\mathbf{x}, t) \tag{8}$$

Moreover, if the loads in the right-hand side of (8) are of the form

$$\begin{cases} \mathbf{b} = \delta(t)\delta(\mathbf{x}-\xi)\mathbf{e}_j \\ q = 0 \end{cases} \quad \text{and} \quad \begin{cases} \mathbf{b} = \mathbf{0} \\ q = -\delta(t)\delta(\mathbf{x}-\xi) \end{cases} \tag{9}$$

the governing differential equations become

$$\mathbf{L}(\nabla, \partial_t)\mathbf{U}(\mathbf{x}, t) = \delta(t)\delta(\mathbf{x})\mathbf{I} \tag{10}$$

where $\mathbf{e}_j$ is a unit vector, $\delta(t)$ is the Dirac delta-function, $\delta(\mathbf{x}) = \delta(x_1)\delta(x_2)\delta(x_3)$, and $\mathbf{I}$ is the 4×4 unit matrix.

There are various ways of solving (10). One way is by representing $\delta(\mathbf{x})$ and $\mathbf{U}(\mathbf{x}, t)$ in terms of integrals over the unit sphere $|\mathbf{n}| = 1$, in which case the fundamental solutions become

$$U_{iM}(\mathbf{x}, t) = -\frac{H(t)}{4\pi^2}\frac{\partial}{\partial t}\int_{|\mathbf{n}|=1}\sum_{\lambda_k>0}\delta(\Lambda_k)\operatorname*{res}_{\lambda=\lambda_k}\left\{\frac{N_{ij}^{-1}(\mathbf{n}, \lambda)}{\lambda^{-2}}\right\}F_{jM}(\mathbf{n})\,\mathrm{d}\Omega(\mathbf{n}) \tag{11a}$$

$$U_{4M}(\mathbf{x}, t) = -\frac{H(t)}{4\pi^2}\frac{\partial}{\partial t}\int_{|\mathbf{n}|=1}\sum_{\lambda_k>0}\delta(\Lambda_k)\operatorname*{res}_{\lambda=\lambda_k}\left\{\frac{N_{ij}^{-1}(\mathbf{n}, \lambda)}{\lambda^{-2}}\right\}\frac{F_{jM}(\mathbf{n})a_i(\mathbf{n})}{\alpha(\mathbf{n})}\,\mathrm{d}\Omega(\mathbf{n}) - \frac{\delta(t)\delta_{4M}}{4\pi\sqrt{\kappa(\mathbf{x})}} \tag{11b}$$

where $\mathrm{d}\Omega(\mathbf{n})$ is the sphere's surface element, and

$$\Lambda_k = t - \mathbf{x}\cdot\frac{\mathbf{n}}{\lambda_k}, \quad \kappa(\mathbf{x}) = \varepsilon_{ik}^c x_i x_k \tag{12}$$

where λ_k are the wave speeds of the material and ε_{ik}^c are the cofactors of the dielectric tensor ε_{ik}.

Thus, (11a) represents the three components of the displacement $\mathbf{u}$ when point forces ($M = 1, 2, 3$) or point charges ($M = 4$) are applied at the source point, while (11b) gives the electric potential response to those same loads. In (11)

$$\begin{aligned} F_{jM}(\mathbf{n}) &= \delta_{jM} + \frac{a_j}{\alpha}\delta_{4M} \\ N_{ij}(\mathbf{n}, \lambda) &= \rho\lambda^2\delta_{ij} - B_{ij}(\mathbf{n}) \\ B_{ij}(\mathbf{n}) &= A_{ij} + \frac{a_i a_j}{\alpha} \end{aligned} \tag{13}$$

and N_{ij}^{-1} are the components of the inverse of N_{ij}. Furthermore, δ_{jM} is the Kronecker delta. Generalizing a terminology common in elastodynamics we shall call $\mathbf{N}(\mathbf{n}, \lambda)$ the electro-acoustic tensor for a plane wave propagating in the direction of $\mathbf{n}$ with speed λ.

3. Green's functions representation via slowness surfaces

It turns out that representations like those given by (11) are not convenient from a computational point of view. Indeed, numerical integration of the delta-function is not trivial, even over a simple surface like the sphere since there are three wave speeds for every single direction of $\mathbf{n}$.

An alternate representation stems from a coordinate transformation that maps the unit sphere into the material's slowness surface S, which consists of three smooth and closed sheets S_1, S_2 and S_3 (i.e. $S = \bigcup_{j=1}^{3} S_j$) enclosing the origin. To this end let us consider the slowness vector $\mathbf{s}$ such that, for each sheet S_j,

$$\mathbf{s} = \frac{\mathbf{n}}{\lambda_j(\mathbf{n})}, \quad \mathbf{s} \in S_j \tag{14}$$

Furthermore, by (13) the slowness surface can be expressed as

$$Q(\mathbf{s}) = \det \mathbf{N}(\mathbf{s}, 1) = 0 \tag{15}$$

The shapes of the slowness sheets depend on the material properties. For example, for crystals of the class 6 mm and for transversely isotropic piezoceramics (poled in the x_3-direction), the sheets are three 'concentric' distorted ellipsoids whose traces are shown in Fig. 1 for three different ceramics. In the limit of isotropy the ellipsoids collapse into a single sphere. It is important to note that ceramics with slightly different chemical compositions may have quite different slowness surfaces and therefore, substantially different electro-acoustic responses. For example, in Fig. 1(a) we show the three, clearly convex, slowness sheets corresponding to a PZT-4 ceramic (Berlincourt et al., 1964). In contrast, a PZT-5 ceramic yields the slowness sheets shown in Fig. 1(b), where it can be observed that the second sheet S_2 has almost vanishing curvature at $x_3 = 0$, however, the whole surface remains convex. Quite different are the features of the slowness sheets shown in Fig. 1(c), which correspond to a Titanate–Lead–Zirconate ceramic manufactured by Quartz and Silice (1995) whose second slowness sheet is not convex. The issue of convexity and how it affects the present formulation is the subject of a separate forthcoming article. We, however, do provide at the end of this section highlights on how piezoelectric slowness surfaces are represented.

Mapping the Green's functions onto the slowness surface reduces (11) to

$$U_{iM}(\mathbf{x}, t) = \frac{H(t)}{4\pi^2} \frac{\partial}{\partial t} \int_{Q=0} \frac{\operatorname{sgn}(\mathbf{s} \cdot \nabla Q) P_{ij}(\mathbf{s}) F_{jM}(\mathbf{s}) \delta(t - \mathbf{x} \cdot \mathbf{s})}{|\nabla Q|} \mathrm{d}S(\mathbf{s}) \tag{16a}$$

$$U_{4M}(\mathbf{x}, t) = \frac{H(t)}{4\pi^2} \frac{\partial}{\partial t} \int_{Q=0} \frac{\operatorname{sgn}(\mathbf{s} \cdot \nabla Q) a_i(\mathbf{s}) P_{ij}(\mathbf{s}) F_{jM}(\mathbf{s}) \delta(t - \mathbf{x} \cdot \mathbf{s})}{\alpha(\mathbf{s}) |\nabla Q|} \mathrm{d}S(\mathbf{s}) - \frac{\delta(t) \delta_{4M}}{4\pi \sqrt{\kappa(\mathbf{x})}} \tag{16b}$$

where $\operatorname{sign}(\cdot)$ is the signum function and

$$\mathbf{P}(\mathbf{s}) = Q(\mathbf{s}) \mathbf{N}^{-1}(\mathbf{s}, 1) \tag{17}$$

is the matrix of the cofactors of $\mathbf{N}(\mathbf{s}, 1)$. Let us point out that while the use of slowness surfaces is certainly well known in anisotropic elastodynamics to describe physical properties or characteristics of a material (e.g. Musgrave, 1970; Abbudi and Barnett, 1991), the representation of the piezoelectric Green's function over such surfaces was introduced for the first time by Khutoryansky and Sosa (1995).

The propagation of a disturbance in the material can be expressed by the intersection of the slowness surface S with the plane $\mathbf{x} \cdot \mathbf{s} = t$ (representing the disturbance), which moves in the direction of $\mathbf{x}$ with unit speed. Such intersection line, which is shown schematically in Fig. 1(a), is thus given by

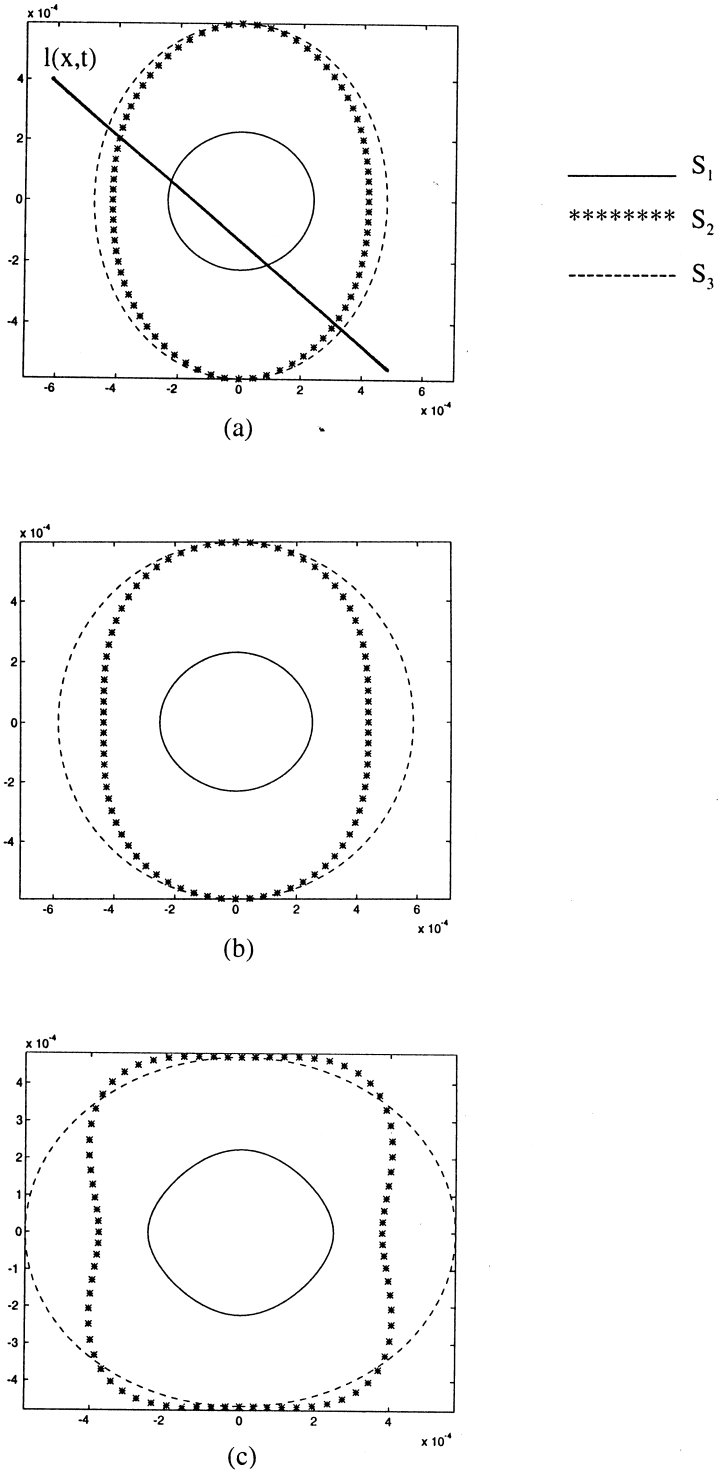

Fig. 1. Slowness sheets for: (a) PZT-4; (b) PZT-5; (c) TiPbZi. Poling direction coincides with the vertical axis.

$$l(\mathbf{x}, t) = \{Q(\mathbf{s}) = 0\} \bigcap \{\mathbf{x} \cdot \mathbf{s} = t\} \tag{18}$$

It is in terms of integrals over such lines that the dynamic electro-elastic Green's functions can be represented with substantial benefits as is shown in the next section.

Before closing this section let us elaborate further on the characteristics and the representation of the slowness surfaces shown in Fig. 1. We rewrite the equation for the slowness surface as

$$Q(\mathbf{s}) = Q_1(\mathbf{s})Q_2(\mathbf{s})Q_3(\mathbf{s}) \tag{19}$$

where

$$Q_1(\mathbf{s})Q_2(\mathbf{s}) = N_{11}(\mathbf{s}', 1)N_{33}(\mathbf{s}', 1) - N_{13}^2(\mathbf{s}', 1) \tag{20a}$$

$$Q_3(\mathbf{s}) = \rho - A_{22}(\mathbf{s}') \tag{20b}$$

and

$$s_1' = \sqrt{s_1^2 + s_2^2}, \quad s_2' = 0, \quad s_3' = s_3 \tag{21}$$

It turns out that one can separate $Q_1(\mathbf{s})$ and $Q_2(\mathbf{s})$ by using the explicit form of the wave speeds, which are deduced by combining (13) and (15) yielding

$$\lambda_{1,2}(\mathbf{n}) = \frac{1}{\sqrt{\rho}} \left\{ \frac{1}{2} [B_{11}(\mathbf{n}') + B_{33}(\mathbf{n}')] \pm \sqrt{1/4[B_{11}(\mathbf{n}') + B_{33}(\mathbf{n}')]^2 + B_{13}^2(\mathbf{n}')} \right\}^{1/2} \tag{22}$$

where the components of $\mathbf{n}'$ are given by

$$n_1' = \sqrt{n_1^2 + n_2^2}, \quad n_2' = 0, \quad n_3' = n_3 \tag{23}$$

Next, to represent each sheet S_j we introduce a spherical coordinate system, such that

$$s_1 = r \sin\theta \cos\phi, \quad s_2 = r \sin\theta \sin\phi, \quad s_3 = r \cos\phi \tag{24}$$

where θ is the angle between the position vector and the symmetry axes s_3. We note that for every sheet S_j, the corresponding radius r is a function of θ only, that is

$$r = r_j(\theta) = \frac{1}{\lambda_j(\theta)} \tag{25}$$

Moreover, for the materials under consideration, the surface S_3 (represented by $Q_3(\mathbf{s}) = 0$) is an ellipsoid, while S_1 and S_2 remain convex if and only if

$$\frac{\mathrm{d}^2 \lambda_j(\theta)}{\mathrm{d}\theta^2} + \lambda_j > 0; \quad j = 1, 2 \tag{26}$$

The above condition guarantees that for any direction of the observation vector $\mathbf{x}$, there is only one value of t for which the plane $\mathbf{x} \cdot \mathbf{s} = t$ is tangent to S_j. We denote such value by $t_j(\mathbf{x})$ and the corresponding point on S_j by $s_j^*(\mathbf{x})$. Now, if $0 < t < t_j$, then the intersection of the plane $\mathbf{x} \cdot \mathbf{s} = t$ with the surface S_j is a simple closed curve, whose parametric representation can be easily obtained from (25) and (26). In particular, when $x_1^2 + x_2^2 > 0$, this representation is of the form

$$r = r_j(\theta), \quad \phi = \pm\phi_j(\theta), \quad \theta_{*j}(\mathbf{x}, t) \leqslant \theta \leqslant \theta_j^*(\mathbf{x}, t)$$

while if $x_1^2 + x_2^2 = 0$, the parametric representation becomes

$$r = r_j(\theta_j^*), \quad -\pi \leqslant \phi \leqslant \pi$$

We note that to obtain $\mathbf{s}_j^*(\mathbf{x})$, $\theta_{*j}(\mathbf{x}, t)$ and $\theta_j^*(\mathbf{x}, t)$ we need to solve (via simple computational procedures) eight-order algebraic equations.

4. The line integral representation

The integrals given by (16) are at this point simpler to be evaluated than (11). However, one extra degree of simplification can be achieved by a second coordinate transformation, namely we decompose the slowness surface element into two directions perpendicular to each other and tangent to the surface $Q(\mathbf{s}) = 0$, such that $\mathrm{d}S(\mathbf{s}) = \mathrm{d}l(\mathbf{s})\,\mathrm{d}m(\mathbf{s})$, where $\mathrm{d}l$ and $\mathrm{d}m$ are line elements. In addition, noting that

$$\frac{\partial(\mathbf{x}\cdot\mathbf{s})}{\partial\mathbf{m}} = \frac{\sqrt{|\mathbf{x}|^2|\nabla Q|^2 - (\mathbf{x}\cdot\nabla Q)^2}}{|\nabla Q|}$$

where $\mathbf{m}$ is the unit vector tangent to the element $\mathrm{d}m$, the Green's functions can be represented as one-dimensional integrals, namely

$$U_{iM}(\mathbf{x}, t) = \frac{H(t)}{4\pi^2}\frac{\partial}{\partial t}\int_{l(x,t)} \frac{\mathrm{sgn}(\mathbf{s}\cdot\nabla Q)P_{ij}(\mathbf{s})F_{jM}(\mathbf{s})}{\sqrt{|\mathbf{x}|^2|\nabla Q|^2 - (\mathbf{x}\cdot\nabla Q)^2}}\mathrm{d}l(\mathbf{s}) \tag{27a}$$

$$U_{4M}(\mathbf{x}, t) = \frac{H(t)}{4\pi^2}\frac{\partial}{\partial t}\int_{l(x,t)} \frac{\mathrm{sgn}(\mathbf{s}\cdot\nabla Q)a_i(\mathbf{s})P_{ij}(\mathbf{s})F_{jM}(\mathbf{s})}{\alpha(\mathbf{s})\sqrt{|\mathbf{x}|^2|\nabla Q|^2 - (\mathbf{x}\cdot\nabla Q)^2}}\mathrm{d}l(\mathbf{s}) - \frac{\delta(t)\delta_{4M}}{4\pi\sqrt{\kappa(\mathbf{x})}} \tag{27b}$$

where $l(\mathbf{x}, t)$ is the intersection line given by (18).

Note that not only the representation of the fundamental solution is effected over a line integral, but also that the delta function has been eliminated altogether from this representation with obvious benefits from a computational point of view.

Since in this article we are interested in sources of electric nature, let us consider the case when the subscript M in (27) takes the value $M = 4$. Accordingly, we write:

$$U_{iM} = U_{i4} = u_i; \quad U_{4M} = U_{44} = \phi;$$

$$F_{jM} = F_{j4} = F_j = \frac{a_j}{\alpha}$$

and (27) becomes

$$u_i(\mathbf{x}, t) = \frac{H(t)}{4\pi^2}\frac{\partial}{\partial t}\int_{l(x,t)} \frac{\mathrm{sgn}(\mathbf{s}\cdot\nabla Q)P_{ij}(\mathbf{s})a_j(\mathbf{s})}{\alpha(\mathbf{s})\sqrt{|\mathbf{x}|^2|\nabla Q|^2 - (\mathbf{x}\cdot\nabla Q)^2}}\mathrm{d}l(\mathbf{s}) \tag{28a}$$

$$\phi(\mathbf{x},t)=\frac{H(t)}{4\pi^2}\frac{\partial}{\partial t}\int_{l(x,t)}\frac{\operatorname{sgn}(\mathbf{s}\cdot\nabla Q)a_i(\mathbf{s})P_{ij}(\mathbf{s})a_j(\mathbf{s})}{\alpha^2(\mathbf{s})\sqrt{|\mathbf{x}|^2|\nabla Q|^2-(\mathbf{x}\cdot\nabla Q)^2}}\,\mathrm{d}l(\mathbf{s})-\frac{\delta(t)}{4\pi\sqrt{\kappa(\mathbf{x})}} \tag{28b}$$

We can test the validity of these equations by analyzing its behavior in the limiting case of isotropic materials. Under such circumstances, piezoelectricity is absent (i.e. $a_j=0$), thus no deformations are induced and the electric potential reduces to

$$\phi(\mathbf{x},t)=\frac{-\delta(t)}{4\pi\varepsilon_0|\mathbf{x}|}=\frac{-\delta(t)}{4\pi\varepsilon_0(x_ix_i)^{1/2}}$$

as expected according to classical electrostatics.

5. Electric sources of arbitrary shape

The fundamental solutions $\mathbf{U}(\mathbf{x},t)$ have been obtained by assuming the sources to be delta-functions in space and time. Such loads are convenient from a mathematical point of view, but hardly can they be considered as representations of physically realistic loading conditions. Thus, the next natural step is to derive expressions for the Green's functions when the sources are of arbitrary shape. To this end let the fundamental solutions (16) be expressed in the following manner:

$$U_{LM}(\mathbf{x},t)=H(t)\frac{\partial}{\partial t}\int_{Q=0}R_{LM}(\mathbf{s})\delta(t-\mathbf{x}\cdot\mathbf{s})\,\mathrm{d}S(\mathbf{s}) \tag{29}$$

where $R_{LM}(\mathbf{s})$ has the following component form:

$$R_{iM}(\mathbf{s})=\frac{\operatorname{sgn}(\mathbf{s}\cdot\nabla Q)}{4\pi^2|\nabla Q|}P_{ij}(\mathbf{s})F_{jM}(\mathbf{s})\quad\text{or } R_{4M}(\mathbf{s})=\frac{\operatorname{sgn}(\mathbf{s}\cdot\nabla Q)}{4\pi^2|\nabla Q|}\frac{a_i(\mathbf{s})}{\alpha(\mathbf{s})}P_{ij}(\mathbf{s})F_{jM}(\mathbf{s})$$

according to whether displacements or electric potential are being sought. Notice that for the latter case, we omit the second term of (16b) since it bears no impact on the developments presented in the sequel.

Next, suppose that the applied impulsive load is of arbitrary shape in time and is represented by a continuous function $\varphi(t)$ with finite piecewise continuous derivative $\dot{\varphi}(t)$. In such a case, the Green's functions can be represented as the convolution

$$U_{LM}(\mathbf{x},t)*\varphi(t)=\int_{-\infty}^{\infty}U_{LM}(\mathbf{x},\tau)\varphi(t-\tau)\,\mathrm{d}\tau \tag{30}$$

However, this convolution can be represented in a more convenient form: substitution of (29) into the right-hand side of (30) gives

$$U_{LM}(\mathbf{x},t)*\varphi(t)=\int_{Q=0}R_{LM}(\mathbf{s})\int_0^{\infty}\varphi(t-\tau)\dot{\delta}(\tau-\mathbf{x}\cdot\mathbf{s})\,\mathrm{d}\tau\,\mathrm{d}S(\mathbf{s}) \tag{31}$$

and since

$$\int_0^\infty \varphi(t-\tau)\dot{\delta}(\tau-\mathbf{x}\cdot\mathbf{s})\,\mathrm{d}\tau = -\delta(\mathbf{x}\cdot\mathbf{s})\varphi(t)+H(\mathbf{x}\cdot\mathbf{s})\dot{\varphi}(t-\mathbf{x}\cdot\mathbf{s})$$

the convolution (31) becomes

$$U_{LM}(\mathbf{x},t)*\varphi(t) = -\varphi(t)\int_{Q=0} R_{LM}(\mathbf{s})\delta(\mathbf{x}\cdot\mathbf{s})\,\mathrm{d}S(\mathbf{s})+\int_{Q=0} R_{LM}(\mathbf{s})H(\mathbf{x}\cdot\mathbf{s})\dot{\varphi}(t-\mathbf{x}\cdot\mathbf{s})\,\mathrm{d}S(\mathbf{s}) \tag{32}$$

The first integral in (32) is the fundamental solution for the corresponding static problem, which we shall denote by $-U^S_{LM}(\mathbf{x})$. Therefore, we can write

$$U_{LM}(\mathbf{x},t)*\varphi(t) = \varphi(t)U^S_{LM}(\mathbf{x})+\int_{Q=0} R_{LM}(\mathbf{s})H(\mathbf{x}\cdot\mathbf{s})\dot{\varphi}(t-\mathbf{x}\cdot\mathbf{s})\,\mathrm{d}S(\mathbf{s}) \tag{33}$$

or more explicitly,

$$U_{iM}(\mathbf{x},t)*\varphi(t) = \varphi(t)U^S_{iM}(\mathbf{x})+\int_{Q=0} R_{iM}(\mathbf{s})H(\mathbf{x}\cdot\mathbf{s})\dot{\varphi}(t-\mathbf{x}\cdot\mathbf{s})\,\mathrm{d}S(\mathbf{s}) \tag{34a}$$

$$U_{4M}(\mathbf{x},t)*\varphi(t) = \varphi(t)U^S_{4M}(\mathbf{x})+\int_{Q=0} R_{4M}(\mathbf{s})H(\mathbf{x}\cdot\mathbf{s})\dot{\varphi}(t-\mathbf{x}\cdot\mathbf{s})\,\mathrm{d}S(\mathbf{s}) \tag{34b}$$

which is a useful manner of separating quasi-static (given by the product of the function $\varphi(t)$ and the static solution) from transient dynamic effects.

From the point of view of the design of electromechanical devices, knowledge of stress and electric field (or induction) levels caused by sudden loads is of utmost importance. These quantities can be calculated by means of the constitutive equations once the displacements and electric potential are known. For linear piezoelectricity the constitutive equations are given by

$$\begin{aligned}\sigma_{ij} &= C_{ijkl}\frac{\partial u_k}{\partial x_l}+e_{kij}\frac{\partial \phi}{\partial x_k}\\ D_i &= e_{ikl}\frac{\partial u_k}{\partial x_l}-\varepsilon_{ik}\frac{\partial \phi}{\partial x_k}\end{aligned} \tag{35}$$

which in terms of the derivatives of the fundamental solutions can be expressed as

$$S_{ijM}(\mathbf{x},t;\varphi) = C_{ijkl}\frac{\partial U_{kM}}{\partial x_l}(\mathbf{x},t)*\varphi(t)+e_{kij}\frac{\partial U_{4M}}{\partial x_k}(\mathbf{s},t)*\varphi(t) \tag{36a}$$

$$S_{4iM}(\mathbf{x},t;\varphi) = e_{ikl}\frac{\partial U_{kM}}{\partial x_l}(\mathbf{x},t)*\varphi(t)-\varepsilon_{ik}\frac{\partial U_{4M}}{\partial x_k}(\mathbf{s},t)*\varphi(t) \tag{36b}$$

where the meaning of the variables S_{KLM} $(K,L=i,4)$ should be clear from the definitions of the Green's functions introduced in (4).

Straightforward differentiation of (33) yields

$$\frac{\partial U_{LM}(\mathbf{x},t)}{\partial x_k} * \varphi(t) = \varphi(t)\frac{\partial U^S_{LM}(\mathbf{x})}{\partial x_k} + \int_{Q=0} R_{LM}(\mathbf{s})\delta(\mathbf{x}\cdot\mathbf{s})s_k\dot{\varphi}(t-\mathbf{x}\cdot\mathbf{s})\,\mathrm{d}S(\mathbf{s}) - \int_{Q=0} R_{LM}(\mathbf{s})H(\mathbf{x}\cdot\mathbf{s})s_k\ddot{\varphi}(t-\mathbf{x}\cdot\mathbf{s})\,\mathrm{d}S(\mathbf{s})$$

But

$$\int_{Q=0} R_{LM}(\mathbf{s})\delta(\mathbf{x}\cdot\mathbf{s})s_k\dot{\varphi}(t-\mathbf{x}\cdot\mathbf{s})\,\mathrm{d}S(\mathbf{s}) = \dot{\varphi}(t)\int_{Q=0} R_{LM}(\mathbf{s})\delta(\mathbf{x}\cdot\mathbf{s})s_k\,\mathrm{d}S(\mathbf{s}) = 0$$

because $Q = 0$ is symmetric with respect to the origin, $R_{LM}(\mathbf{s}) = R_{LM}(-\mathbf{s})$ and $\delta(\mathbf{x}\cdot\mathbf{s}) = \delta(-\mathbf{x}\cdot\mathbf{s})$. Hence

$$\frac{\partial U_{iM}(\mathbf{x},t)}{\partial x_k} * \varphi(t) = \varphi(t)\frac{\partial U^S_{iM}(\mathbf{x})}{\partial x_k} - \int_{Q=0} R_{iM}(\mathbf{s})s_k H(\mathbf{x}\cdot\mathbf{s})\ddot{\varphi}(t-\mathbf{x}\cdot\mathbf{s})\,\mathrm{d}S(\mathbf{s}) \tag{37a}$$

$$\frac{\partial U_{4M}(\mathbf{x},t)}{\partial x_k} * \varphi(t) = \varphi(t)\frac{\partial U^S_{4M}(\mathbf{x})}{\partial x_k} - \int_{Q=0} R_{4M}(\mathbf{s})s_k H(\mathbf{x}\cdot\mathbf{s})\ddot{\varphi}(t-\mathbf{x}\cdot\mathbf{s})\,\mathrm{d}S(\mathbf{s}) \tag{37b}$$

where the static derivatives can be written more explicitly as

$$\frac{\partial U^S_{iM}(\mathbf{x})}{\partial x_k} = -\frac{x_j}{8\pi^2|\mathbf{x}|^3}\int_{l_1(\mathbf{x})}\frac{\partial}{\partial n_j}[n_k B^{-1}_{il}(\mathbf{n})F_{lM}(\mathbf{n})]\,\mathrm{d}l(\mathbf{n}) \tag{38a}$$

$$\frac{\partial U^S_{4M}(\mathbf{x})}{\partial x_k} = -\frac{x_j}{8\pi^2|\mathbf{x}|^3}\int_{l_1(\mathbf{x})}\frac{\partial}{\partial n_j}\left[n_k B^{-1}_{il}(\mathbf{n})F_{lM}(\mathbf{n})\frac{a_i(\mathbf{n})}{\alpha(\mathbf{n})}\right]\mathrm{d}l(\mathbf{n}) + \frac{\delta_{4M}\varepsilon^c_{kj}x_j}{4\pi[\varepsilon^c_{ik}x_i x_k]^{3/2}} \tag{38b}$$

where $l_1(\mathbf{x})$ is the intersection of the unit sphere $|\mathbf{n}| = 1$ with the stationary plane $\mathbf{x}\cdot\mathbf{n} = 0$.

When the load is electric in nature, $M = 4$ and (36) reduce to

$$\sigma_{ij}(\mathbf{x},t;\varphi) = C_{ijkl}\frac{\partial u_k}{\partial x_l}(\mathbf{x},t) * \varphi(t) + e_{kij}\frac{\partial \phi}{\partial x_k}(\mathbf{s},t) * \varphi(t) \tag{39a}$$

$$D_i(\mathbf{x},t;\varphi) = e_{ikl}\frac{\partial u_k}{\partial x_l}(\mathbf{x},t) * \varphi(t) - \varepsilon_{ik}\frac{\partial \phi}{\partial x_k}(\mathbf{s},t) * \varphi(t) \tag{39b}$$

where $u_{k,l} * \varphi(t)$ and $\phi_{,k} * \varphi(t)$ are obtained from (37) by setting $M = 4$.

6. Electric sources of triangular shape

Electric pulses occurring in many practical situations can be represented accurately by triangular functions which are the 'least smooth' continuous functions from a mathematical point of view and yet very amenable to numerical treatment. The present section is devoted to such functions. To this end consider the function $\varphi(t)$ given by

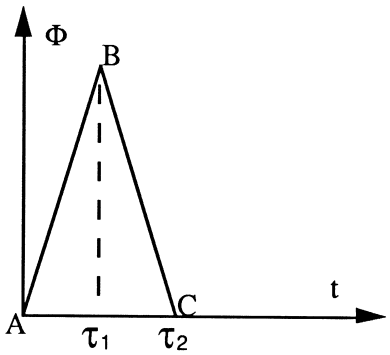

Fig. 2. Pulse of triangular shape.

$$\varphi(t) = \varphi_0 \Phi(t; \tau_1, \tau_2) \tag{40}$$

where φ_0 is the magnitude of the pulse and

$$\Phi(t; \tau_1, \tau_2) = \frac{t}{\tau_1} H(t) - \frac{\tau_2 (t-\tau_1)}{\tau_1 (\tau_2 - \tau_1)} H(t-\tau_1) + \frac{(t-\tau_2)}{(\tau_2 - \tau_1)} H(t-\tau_2) \tag{41}$$

where the time parameters τ_1 and τ_2 determine the front and rear parts of the pulse shown in Fig. 2.

Next we note that on the grid $t_0 < t_1 < \cdots < t_N < t_{N+1}$ a continuous piecewise linear function $f(t)$ can be represented in the interval (t_1, t_N) as

$$f(t) = \sum_{k=1}^{N} f(t_k) \Phi(t; t_k - t_{k-1}, t_{k+1} - t_k)$$

To determine stresses and electric fields (or induction) one needs to calculate the displacement and electric potential gradients which in turn involve second time derivatives of $\varphi(t)$. Using (41) we obtain

$$\ddot{\Phi}(t, \tau_1, \tau_2) = \frac{\delta(t)}{\tau_1} - \frac{\tau_2 \delta(t-\tau_1)}{\tau_1 (\tau_2 - \tau_1)} + \frac{\delta(t-\tau_2)}{\tau_2 - \tau_1} \tag{42}$$

Therefore, for unit impulses ($\varphi_0 = 1$) and after mapping (37) into the line integral we obtain

$$\begin{aligned} \frac{\partial U_{LM}(\mathbf{x}, t)}{\partial x_k} * \Phi(t; \tau_1, \tau_2) = \Phi(t; \tau_1, \tau_2) \frac{\partial U^S_{LM}(\mathbf{x})}{\partial x_k} - \frac{H(t)}{\tau_1} \int_{l(\mathbf{x},t)} Z_{LMk}(\mathbf{x}, \mathbf{s}) \, \mathrm{d}l(\mathbf{s}) \\ + \frac{\tau_2 H(t-\tau_1)}{\tau_1 (\tau_2 - \tau_1)} \int_{l(\mathbf{x},t-\tau_1)} Z_{LMk}(\mathbf{x}, \mathbf{s}) \, \mathrm{d}l(\mathbf{s}) - \frac{H(t-\tau_2)}{\tau_2 - \tau_1} \int_{l(\mathbf{x},t-\tau_2)} Z_{LMk}(\mathbf{x}, \mathbf{s}) \, \mathrm{d}l(\mathbf{s}) \end{aligned} \tag{43}$$

where

$$Z_{LMk}(\mathbf{x},\mathbf{s}) = \frac{|\nabla Q| R_{LM}(\mathbf{s}) s_k}{\sqrt{|\mathbf{x}|^2 |\nabla Q|^2 - (\mathbf{x}\cdot\nabla Q)^2}} \tag{44}$$

In particular, when $M = 4$ the displacement and electric potential gradients are given by

$$\frac{\partial u_i(\mathbf{x},t)}{\partial x_k} * \Phi(t;\tau_1,\tau_2) = \Phi(t;\tau_1,\tau_2)\frac{\partial u_i^S(\mathbf{x})}{\partial x_k} - \frac{H(t)}{\tau_1}\int_{l(\mathbf{x},t)} Z_{ik}(\mathbf{x},\mathbf{s})\,\mathrm{d}l(\mathbf{s}) + \frac{\tau_2 H(t-\tau_1)}{\tau_1(\tau_2-\tau_1)}\int_{l(\mathbf{x},t-\tau_1)} Z_{ik}(\mathbf{x},\mathbf{s})\,\mathrm{d}l(\mathbf{s}) - \frac{H(t-\tau_2)}{\tau_2-\tau_1}\int_{l(\mathbf{x},t-\tau_2)} Z_{ik}(\mathbf{x},\mathbf{s})\,\mathrm{d}l(\mathbf{s}) \tag{45a}$$

and

$$\frac{\partial \phi(\mathbf{x},t)}{\partial x_k} * \Phi(t;\tau_1,\tau_2) = \Phi(t;\tau_1,\tau_2)\frac{\partial \phi^S(\mathbf{x})}{\partial x_k} - \frac{H(t)}{\tau_1}\int_{l(\mathbf{x},t)} Z_{4k}(\mathbf{x},\mathbf{s})\,\mathrm{d}l(\mathbf{s}) + \frac{\tau_2 H(t-\tau_1)}{\tau_1(\tau_2-\tau_1)}\int_{l(\mathbf{x},t-\tau_1)} Z_{4k}(\mathbf{x},\mathbf{s})\,\mathrm{d}l - \frac{H(t-\tau_2)}{\tau_2-\tau_1}\int_{l(\mathbf{x},t-\tau_2)} Z_{4k}(\mathbf{x},\mathbf{s})\,\mathrm{d}l(\mathbf{s}) \tag{45b}$$

where

$$Z_{ik} = \frac{\mathrm{sgn}(\mathbf{s}\cdot\nabla Q) P_{ij}(\mathbf{s}) a_j(\mathbf{s}) s_k}{\alpha(\mathbf{s})\sqrt{|\mathbf{x}|^2|\nabla Q|^2 - (\mathbf{x}\cdot\nabla Q)^2}} \tag{46a}$$

$$Z_{4k} = \frac{\mathrm{sgn}(\mathbf{s}\cdot\nabla Q) a_i(\mathbf{s}) P_{ij}(\mathbf{s}) a_j(\mathbf{s}) s_k}{\alpha^2(\mathbf{s})\sqrt{|\mathbf{x}|^2|\nabla Q|^2 - (\mathbf{x}\cdot\nabla Q)^2}} \tag{46b}$$

while the static derivatives are obtained from (38) and are given by

$$\frac{\partial u_i^S(\mathbf{x})}{\partial x_k} = -\frac{x_j}{8\pi^2|\mathbf{x}|^3}\int_{l_1(\mathbf{x})}\frac{\partial}{\partial n_j}\left[n_k B_{il}^{-1}(\mathbf{n})\frac{a_l(\mathbf{n})}{\alpha(\mathbf{n})}\right]\mathrm{d}l(\mathbf{n}) \tag{47a}$$

$$\frac{\partial \phi^S(\mathbf{x})}{\partial x_k} = -\frac{x_j}{8\pi^2|\mathbf{x}|^3}\int_{l_1(\mathbf{x})}\frac{\partial}{\partial n_j}\left[n_k B_{il}^{-1}(\mathbf{n})\frac{a_i(\mathbf{n})a_l(\mathbf{n})}{\alpha^2(\mathbf{n})}\right]\mathrm{d}l(\mathbf{n}) + \frac{\varepsilon_{kj}^c x_j}{4\pi[\varepsilon_{ik}^c x_i x_k]^{3/2}} \tag{47b}$$

Notice that if the material is not piezoelectric but remains anisotropic, the coefficients a_i vanish. Therefore, no strains are induced and the electric field components are given by the second term of (47b) which coincides with the results given, for example, by Landau et al. (1984). Moreover, (47b) clearly indicates that piezoelectricity can affect substantially the behavior of an anisotropic dielectric, enhancing or reducing [depending on the sign of the first term in (47b)] the magnitude of the electric field generated by point charges.

7. Numerical results

We consider ceramics of the family PZT-5 (Berlincourt et al., 1964) that have been poled in the x_3-direction. Let the distance between the source of the disturbance and the field (or observation)

point be 10^{-3} m. Furthermore, for purposes of practical application, pulses of symmetric triangular shape and of magnitude 10^{-6} Coulombs are applied [therefore, the expressions given from (43)–(47) must be multiplied by this charge] with durations $2\tau = 0.5 \times 10^{-7}$ s. Moreover, if $c_1(\mathbf{n})$ is the maximum speed of propagation of the piezoelectric strain waves in the $\mathbf{n}$ direction, then the wave length is equal to $2c_1\tau$ and the corresponding frequency has the value $f = 1/2\tau = 20$ MHz.

Since $\tau_2 = 2\tau_1 = 2\tau$, eqn (41) becomes

$$\Phi_\tau(t) = \Phi(t;\tau) = \frac{1}{\tau}[tH(t) - 2(t-\tau)H(t-\tau) + (t-2\tau)H(t-2\tau)] \tag{48}$$

It is of interest to show the behavior of the electro-elastic variables along two mutually perpendicular directions, namely x_1 (the same behavior is observed along the x_2-axis due to the material symmetry of the ceramic) and x_3.

First we consider the induced electric field under time independent conditions. As we know from electrostatics, the electric field generated by a point charge has a radial distribution which emanates from or points towards the charge according to whether the applied charge is positive or negative, respectively. Thus along a coordinate axis with unit vector $\mathbf{e}_i$ the field is given by $\mathbf{E} = E_i\mathbf{e}_i$. If the material is isotropic the field will have the same value (this value being larger in vacuum than in

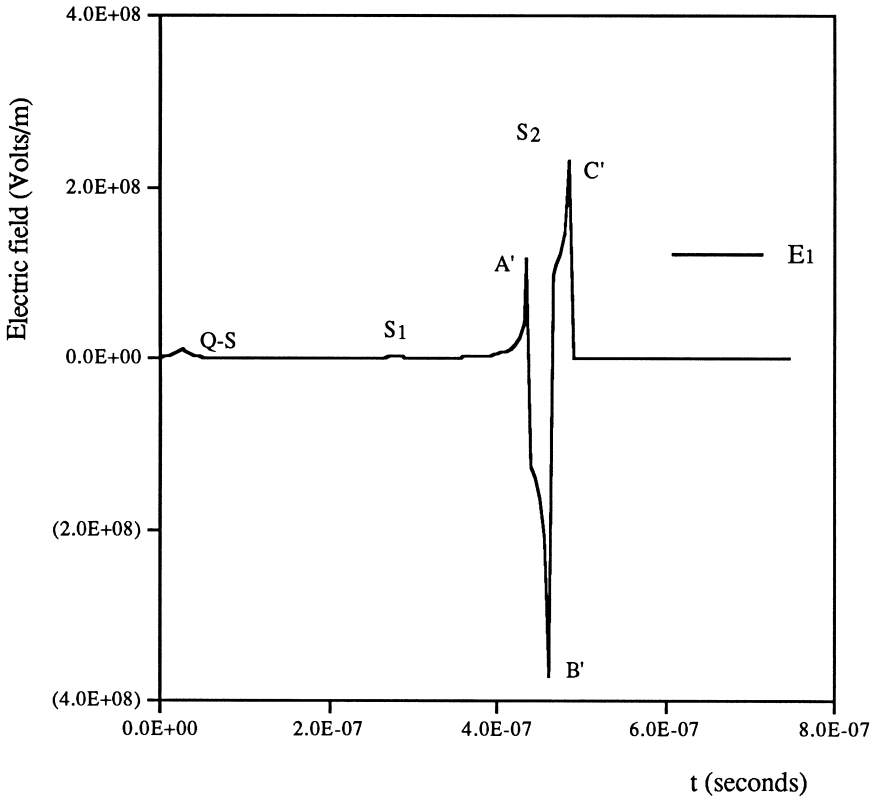

Fig. 3. Electric field induced in x_1-direction.

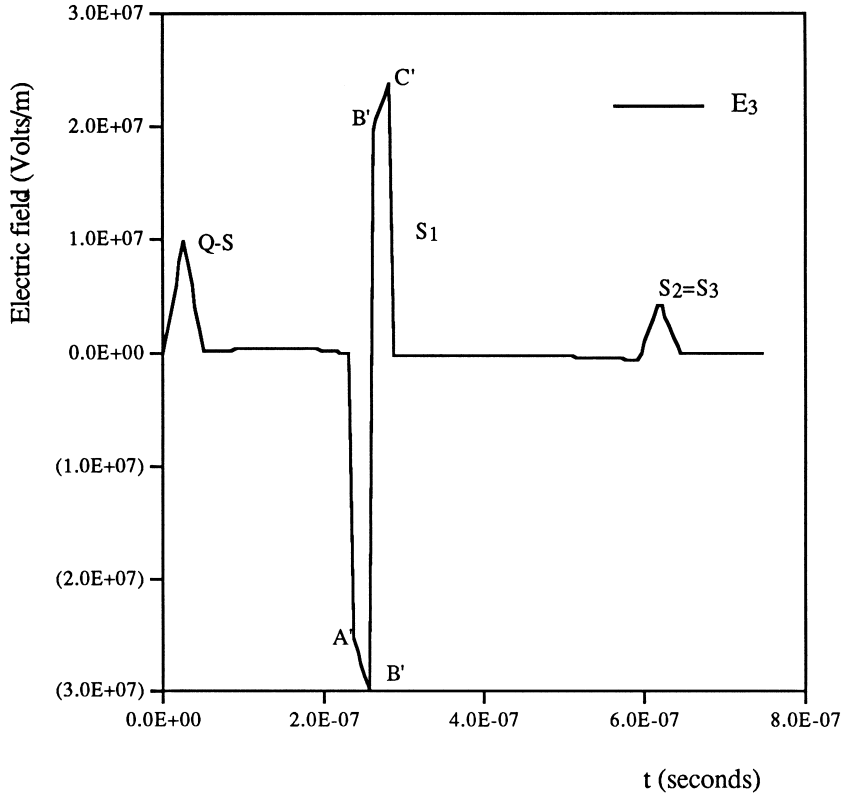

Fig. 4. Electric field induced in x_3-direction.

matter) in any direction at a given point. When the material is not isotropic this is no longer the case. For the piezoceramic under consideration the static values of the field at the distance 10^{-3} m generated by a positive point charge of 1 μC are computed using (47b), which yields $E_1 = 6.74 \times 10^6$ V/m and $E_3 = 5.32 \times 10^6$ V/m, that is $E_1/E_3 = 1.26$. One can go a step further and neglect piezoelectricity altogether, which is a common practice in simplified analysis. The present formulation allows for such approximation by simply setting $a_i = 0$ in (47b), in which case the electric field components have magnitudes $E_1 = 10.31 \times 10^6$ V/m and $E_3 = 9.82 \times 10^6$ V/m, thus $E_1/E_3 = 1.05$. That is, neglecting piezoelectricity not only tends to overestimate the magnitudes of the induced fields but also reduces the effect of anisotropy.

Next, we shift our attention to the characteristics of the induced electric field when the applied charge varies in time according to the pulse shown in Fig. 2. Using (45b) and (46b) we obtain the responses shown in Figs 3 and 4. A few comments are drawn from these figures. First, the maximum values of the fields in the x_1- and x_3-directions are approximately $E_1 = -3.8 \times 10^8$ V/m and $E_3 = -3 \times 10^7$ V/m, that is $E_1/E_3 = 12.6$. Therefore, not only the fields components are much larger than in the static case, but also the difference in magnitudes in two mutually perpendicular directions is much more pronounced than under static conditions. The latter effect is a consequence of the difference in radius of curvature of the slowness sheet S_2 which is much larger at $x_3 = 0$ than

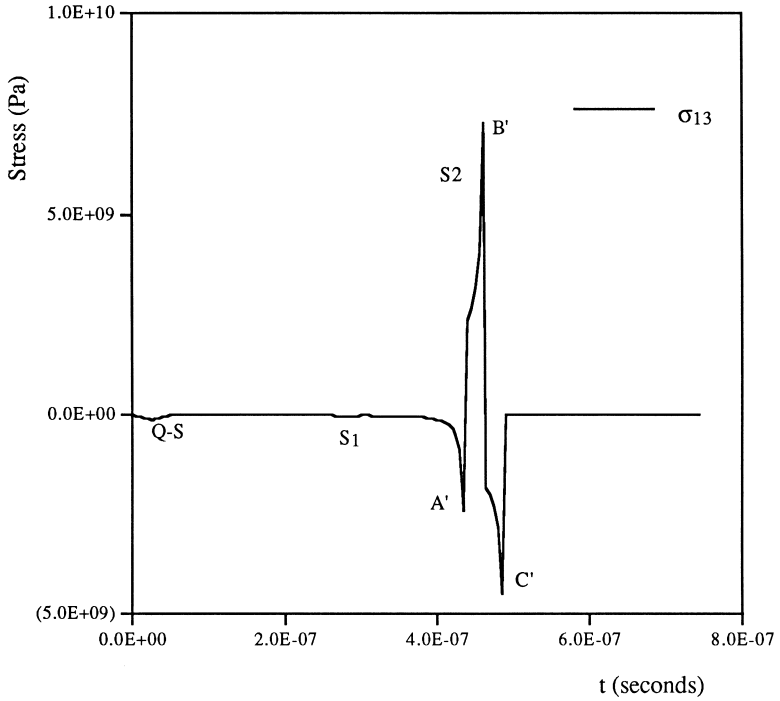

Fig. 5. Shear stress induced in x_1-direction.

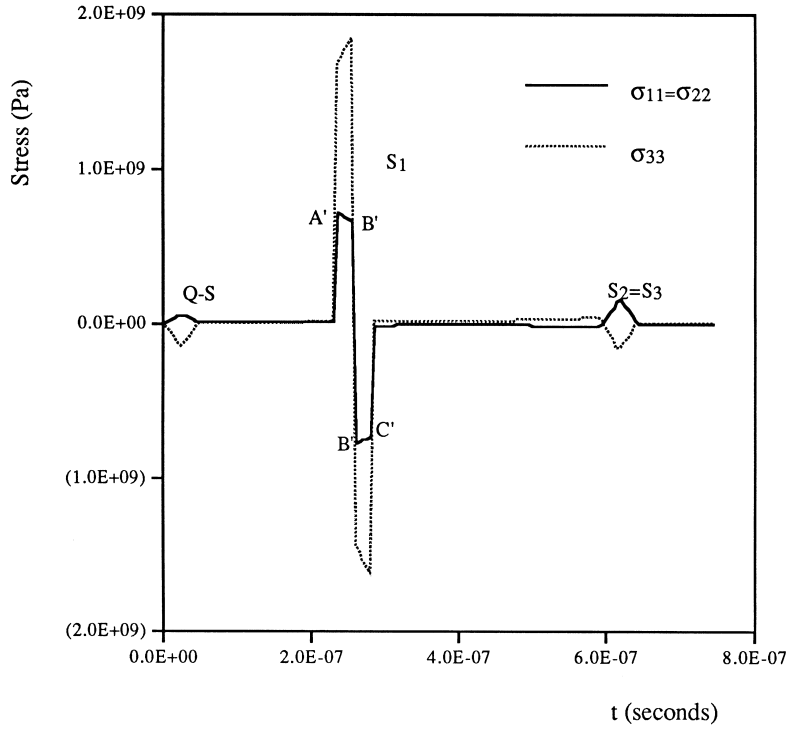

Fig. 6. Normal stress induced in x_3-direction.

at $x_1 = 0$ (in other words, the larger the radius of curvature of the slowness sheet the larger the induced field). Second, it is important to bring to the reader's attention the nature of the various peaks shown in Figs 3 and 4. The first peaks in both figures (denoted by Q-S) are manifestations of the quasi-static solution induced by the purely electrostatic field (that is, without coupling). These pulses propagate with infinite speed and are much smaller in magnitude than the waves induced by piezoelectricity which travel with finite speeds. Finally, the interpretation of the other peaks is done with the aid of Figs 1(b) and 2. In Fig. 3 we indicate by S_1 the very small pulse corresponding to the first slowness sheet at $x_3 = 0$ which occurs at approximately $t = 2.8 \times 10^{-7}$ s. Points A', B' and C' corresponding to the second sheet S_2 (which occurs at approximately $t = 4.4 \times 10^{-7}$ s), correspond to points A, B and C of Fig. 2. Notice that there is no wave associated with the third sheet in the x_1-direction. In Fig. 3 the interpretations are similar, except that all three sheets can be observed. In particular at $x_1 = 0$, $S_2 = S_3$ as can be observed in Fig. 1(b).

Because of piezoelectricity, the applied charge pulse also induces stresses, which are numerically calculated using (45), (46) and the constitutive eqns (39a). The results are shown in Figs 5 and 6 for the x_1- and x_3-directions, respectively. We note that as was the case for the fields, significant induced stresses occur first in the poling direction. Figure 5 indicates that only shear stress σ_{13} is induced, which attains a maximum value of approximately 7.1×10^9 Pa. On the other hand, in the x_3-directions all normal stress are induced with peak values $\sigma_{11} = \sigma_{22} = 0.7 \times 10^9$ Pa and $\sigma_{33} = 1.8 \times 10^9$ Pa. All these peak stresses are substantially much larger than the corresponding tensile and compressive strengths of most industrial piezoceramics, which are in the order of 80 and 600 MPa, respectively. Therefore, we infer that catastrophic failure could certainly occur even at lower levels of electric discharges. The present analysis becomes even more relevant from a structural integrity point of view in more realistic situations where the ceramic tends to be weakened by manufacturing induced defects or metallic surfaces.

Finally, although not shown in this article, we need to mention that there is a strong dependence of the electro-elastic variables response on the frequency of the applied electric pulses: in fact, the larger the duration of the signal (reflected in the parameter τ) the smaller the peak values attained by the induced fields.

8. Conclusions

The transient dynamic response of piezoelectric ceramics subjected to electric discharges has been addressed analytically via the use of Green's functions. Integral representations of these functions have been reduced to integral lines which in turn were solved numerically for a particular case of the time dependent applied electric charge. The results obtained with the aid of these representations are shown to reduce to limiting and well-known cases such as isotropic and anisotropic electrostatics and static piezoelectricity. Moreover, important predictions regarding the electric and mechanical reliability of the ceramic can be made thus avoiding the performance of controlled laboratory experiments.

Acknowledgement

Portions of this work were done during a visit of H.S. to Universidad Nacional de Buenos Aires, Argentina with the support of a Fulbright award.

References

Abbudi, M., Barnett, D., 1991. Three-dimensional computer visualization of the slowness surfaces of anisotropic crystals. In: Wu, J., Ting, T.C.T., Barnett, D. (Eds.), Modern Theory of Anisotropic Elasticity and Applications. SIAM, pp. 290–300.

Berlincourt, D., Curran, D. and Jaffe, H., 1964. Piezoelectric and piezoceramic materials and their function in transducers. In: Mason, W.P. (Ed.), Physical Acoustics, Vol. I-A. Academic Press.

Freiman, S.W., Pohanka, R.C., 1989. Review of mechanically related failures of ceramic capacitors and capacitor material. J. Am. Ceram. Soc. 72, 2258–2263.

Khutoryansky, N., Sosa, H., 1995. Dynamic representation formulas and fundamental solutions for piezoelectricity. Int. J. Solids Struct. 32, 3307–3325.

Landau, L.D., Lifshitz, E.M., Pitaevskii, L.P., 1984. Electrodynamics of Continuous Media. 2nd ed. Pergamon Press, Oxford.

McMeeking, R., 1987. On mechanical stresses at cracks in dielectrics with application to dielectric breakdown. J. Appl. Phys. 62, 3116–3122.

Musgrave, M.J., 1970. Crystal Acoustics. Holden-Day, San Francisco.

Pak, Y.E., 1990. Crack extension force in a piezoelectric material. J. Appl. Mech. 57, 647–653.

Quartz et Silice, 1995. Private communication. Fontanbleu, France.

Sosa, H., 1991. Plane problems in piezoelectric media with defects. Int. J. Solids Struct. 28, 491–505.

Sosa, H., 1992. On the fracture mechanics of piezoelectric solids. Int. J. Solids Struct. 29, 2613–2622.

Sosa, H., Khutoryansky, N., 1996. New developments concerning piezoelectric materials with defects. Int. J. Solids Struct. 33, 3399–3414.

Suo, Z., 1993. Models for breakdown-resistant dielectric and ferroelectric ceramics. J. Mech. Phys. Solids 41, 1155–1176.